Reduced Oxidative Phosphorylation and Increased Glycolysis in Human Glaucoma Lamina Cribrosa Cells

Khalid Kamel,[1] Colm J. O'Brien,[1,3] Alexander V. Zhdanov,[2] Dmitri B. Papkovsky,[2] Abbot F. Clark,[4] Daniel Stamer,[5] and Mustapha Irnaten[1]

[1]Department of Ophthalmology, Mater Misericordiae University Hospital, Dublin, Ireland
[2]School of Biochemistry & Cell Biology, University College Cork, Cork, Ireland
[3]School of Medicine and Medical Science, University College Dublin, Dublin, Ireland
[4]Department of Pharmacology & Neuroscience and the North Texas Eye Research Institute, University of North Texas, Health Science Center, Fort Worth, Texas, United States
[5]Department of Ophthalmology, Duke University, Durham, North Carolina, United States

Correspondence: Mustapha Irnaten, UCD Clinical Research Centre, Mater Misericordiae University Hospital, 21 Nelson Street, Dublin 7, Ireland; mirnaten2014@gmail.com.

Received: April 19, 2020
Accepted: September 25, 2020
Published: November 2, 2020

Citation: Kamel K, O'Brien CJ, Zhdanov AV, et al. Reduced oxidative phosphorylation and increased glycolysis in human glaucoma lamina cribrosa cells. *Invest Ophthalmol Vis Sci.* 2020;61(13):4. https://doi.org/10.1167/iovs.61.13.4

Purpose. The lamina cribrosa (LC) is a key site of damage in glaucomatous optic neuropathy. We previously found that glaucoma LC cells have an increased profibrotic gene expression, with mitochondrial dysfunction in the form of decreased mitochondrial membrane potential. Altered cell bioenergetics have recently been reported in organ fibrosis and in cancer. In this study, we carried out a systematic mitochondrial bioenergetic assessment and measured markers of alternative sources of cellular energy in normal and glaucoma LC cells.

Methods. LC cells from three glaucoma donors and three age-matched normal controls were assessed using VICTOR X4 Perkin Elmer (Waltham, MA) plate reader with different phosphorescent and luminescent probes. adenosine triphosphate levels, oxygen consumption rate, and extracellular acidification were measured and normalized to total protein content. RNA and protein expression levels of *MCT1, MCT4, MTFHD2*, and *GLS2* were quantified using real-time RT-PCR and Western blotting.

Results. Glaucoma LC cells contain significantly less adenosine triphosphate ($P < .05$) when supplied with either glucose or galactose. They also showed significantly diminished oxygen consumption in both basal and maximal respiration with more lactic acid contribution in ECA. Both mRNA and protein expression levels of *MCT1, MCT4, MTHFD2*, and *GLS2* were significantly increased in glaucoma LC cells.

Conclusions. We demonstrate evidence of metabolic reprogramming (The Warburg effect) in glaucoma LC cells. Expression of markers of glycolysis, glutamine, and one carbon metabolism are elevated in glaucoma cells at both the mRNA and protein levels. A better understanding of bioenergetics in glaucoma may help in the development of new therapeutics.

Keywords: glaucoma, mitochondria, lamina cribrosa, Warburg

Glaucoma is an optic neuropathy characterized by the irreversible degeneration of retinal ganglion cell (RGC) axons leading to gradual vision impairment and blindness.[1] Major risk factors are elevated IOP and reduced ocular perfusion.[2] High IOP causes mechanical distortion and stretching of the RGC axons at the lamina cribrosa (LC), obstructing the axoplasmic flow within the axons.[3] This process involves several pathological features such as cupping of the optic nerve head and excessive extracellular matrix (ECM) deposition in the LC region leading to remodeling and fibrosis.[4,5] Tissue healing is an essential mechanism that allows damaged tissues to repair. If this process becomes persistent, ECM and tissue cells accumulate molecular damage and exhibit destructive and dysregulated responses, ultimately leading to increased tissue fibrosis and stiffness.[6]

The molecular hallmarks of fibrosis include fibroblast mitochondrial dysfunction and impaired cell respiration and metabolism. There is considerable evidence of mitochondrial dysfunction and altered cell bioenergetics in various forms of organ fibrosis (cardiac, pulmonary, renal, and skin) and in cancer-associated fibroblasts.[7–9]

Mitochondria have emerged as critical integrators of fundamental cellular processes, ranging from adenosine triphosphate (ATP) production and signal transduction to the maintenance of Ca^{2+} homeostasis, cell proliferation, and apoptosis.[10] They generate ATP through several mechanisms, including most importantly oxidative phosphorylation (OXPHOS), the Krebs cycle, glutaminolysis, and β-oxidation of fatty acids. As each mechanism has a spare capacity in the resting state, several regulatory mechanisms allow the different pathways to compensate for each other under conditions of increased energy demand. Dysregulation of these regulatory mechanisms has been identified in different fibrotic diseases.[11,12]

Monocarboxylate transporters (MCTs), including MCT1 and MCT4, are responsible for moving lactate in and out of cells and thus are critical to the regulation of lactate concentrations and glycolysis.[13,14] Significant associations of upregulated MCT1 and/or MCT4 expression have been reported in many types of tumor cells and fibrotic disorders.[15,16] Methylenetetrahydrofolate dehydrogenase 2 (*MTHFD2*) is an enzyme that functions in the mitochondria to generate formate, which enters the cytoplasm and is incorporated into tetrahydrofolates for one carbon metabolism.[17] Although *MTHFD2* has not been directly implicated in fibrosis, its protein product promotes cell proliferation.[18] Another key metabolic enzyme is glutaminase 2 (GLS2), which converts glutamine to glutamate in glutaminolysis.[19] Blockage of GLS with its specific inhibitor was recently found to significantly inhibit fibroblast proliferation in iatrogenic laryngotracheal stenosis scars.[20]

Several eye conditions have been linked to abnormalities of the mitochondria and its respiratory chain.[21] Also, it is increasingly clear that the pathophysiology of glaucoma involves the activation of profibrotic pathways.[22] We previously reported that human glaucoma LC cells exhibit properties similar to activated myofibroblasts including increased profibrotic ECM gene transcription and protein synthesis (collagen 1A1, periostin, fibronectin),[23] elevated intracellular calcium and reactive oxygen species levels, and increased mitochondrial number with evidence of oxidative stress.[24–26]

With the advent of high-throughput technology in measuring cellular respiration together with the development of specific mitochondrial inhibitors, a detailed bioenergetic profile of cells can be obtained. This profile can help as an early sensor to diagnose and predict the prognosis of various chronic and complex diseases with dysfunctional metabolism.[27,28] In our study, we conducted a detailed mitochondrial bioenergetic assessment on normal and glaucoma LC cells, and the results prompted us to measure markers of alternative sources of cellular energy in this group of cells.

Methods

LC Cells Culture and Characterization

Human glial fibrillary acidic protein–negative normal control and glaucomatous LC cells were isolated and cultured from donor eyes as previously described by Lambert et al.[29] (Alcon Labs, Fort Worth, TX; Duke University, Durham, NC). Freshly thawed primary cells were dissected from healthy donor eyes with no history of glaucoma, ocular disease, or other neurologic diseases ($n = 3$ eye donors) and from age-matched donors with confirmed glaucoma ($n = 3$ eye donors). All eyes were from anonymous donors from regional eye banks, and they were obtained and managed in compliance with the Declaration of Helsinki for research involving human tissue. To characterize LC cells, they were routinely stained positively for α-smooth muscle actin and negatively for both glial fibrillary acidic protein (an astrocyte marker) and ionized Ca^{2+} binding adapter molecule 1 (a microglial marker) as previously described.[24,29,30] Briefly, cells were cultured and maintained at 37°C with 95% humidified air and 5% CO_2, supplemented with 10% (v/v) FBS and 1% L-glutamine–penicillin–streptomycin. Cells were maintained in full medium until reaching 90% confluence and passaged as needed. Cells used in the experiments were in second to eighth passage.

Plate Reader VICTOR X4

The multilabel plate reader used is a VICTOR X4 (PerkinElmer, Waltham, MA) capable of luminescence and absorbance measurements in 96-well plates, equipped with temperature control, red-sensitive photodetector (up to 700 nm), as well as software for kinetic assays and a set of optical filters: excitation for pH-Xtra and MitoXpress–Xtra: 340 to 390 nm, Emission for pH-Xtra: 615 ± 5 nm, Emission for MitoXpress: 640-660 nm, Luminescence (ATP assay): no filter (empty slot, excitation lamp-OFF).

Absorbance (bicinchoninic acid assay [BCA]) was quantified using a multiple microplate reader (Molecular Devices, San Jose, CA; Spectra Max) at a wavelength of 490 nm. The ECA and oxygen consumption (OCR) assays utilize the long-decay photoluminescent probes pH-Xtra and MitoXpress–Xtra (Luxcel Biosciences, Cork, Ireland) and fluorescence lifetime (LT) measurements on a time-resolved fluorescence plate reader. The VICTOR X4 (PerkinElmer) plate reader used here supports this mode and allows rapid LT determination by time-resolved fluorescence intensity measurements at two delay times. Notably, pH-Xtra and MitoXpress-Xtra probes can be used to measure sample pH and dissolved O_2 concentrations, respectively. ATP and total protein are measured with standard chemiluminescence and absorbance based reagents, respectively.

These assays provide detailed information on the cellular metabolic state, with adequate sensitivity and flexibility. So far, the usefulness of this platform has been demonstrated in a number of complex studies performed by different laboratories.[31–33]

Extracellular Acidification (ECA) Assay

Age-matched normal and glaucoma LC cells were seeded at a density of 40,000 cells/well and cultured in a total volume of 100 µL of standard DMEM growth medium supplemented with L-glutamine and antibiotics in a transparent standard flat bottom 96-well plate for 24 hours. On the day of measurement, the plate was incubated in a CO_2-free incubator for 3 hours at 37°C. Subsequently, the medium was carefully removed and replaced with 200 µL/well of fresh DMEM respiration medium containing 10 mM glucose, 2 mM L-glutamine, 1 mM pyruvate, and 20 mM HEPES (4-(2-hydroxyethyl)-1-piperazineethanesulfonic acid) buffer (pH 7.2–7.4). After 30 minutes in CO_2-free conditions, each well was washed with 200 µL of fresh medium (DMEM) 10 mM glucose, 2m M L-glutamine, and 1 mM pyruvate adjusted to pH 7.4 (ECA medium) immediately before the assay. After another 30 minutes, the medium was replaced with 100 µL of the same pH-adjusted medium containing 10 µg of pH probe (pH-Xtra probe, PH-100; Luxcel Biosciences). Prewarmed mineral oil (150 µL at 37°C) was immediately added to wells designated for total-ECA assay (T-ECA), and wells designated for lactate-related ECA (L-ECA) received no mineral oil. The L-ECA assay measures the glycolysis component of medium acidification (i.e., lactate). The T-ECA assay measures acidification owing to both lactate and CO_2 (produced predominantly by the Krebs cycle and pentose phosphate pathway). All assays were conducted in triplicate, including wells with no cells as controls. The plate was inserted immediately to the VICTOR X4 multilabel microplate reader after adjusting temperature to 37°C according to manufacturer's protocol for at least 60 minutes. Readings were taken every 30 seconds.

Investigative Ophthalmology & Visual Science

Phosphorescence LT of pH-Xtra probe increases with [H^+] elevation (or pH reduction).

Total Protein Analysis

Immediately after ECA assay, the ECA medium was removed and lysis buffer was added (Sigma-Aldrich, Arklow, Ireland) to cells in wells designated previously for L-ECA. The plate was put in ice and rotated at 80 rpm for 15 minutes to slow down protein degradation. Cells were then scraped from each well, and each cell lysates were collected in Eppendorf tubes and centrifuged at 14,000*g* for 10 minutes in a chilled centrifuge at 4°C. The cleared supernatant was collected and the protein concentration was quantified using the BCA assay. Aliquots (25 µL) of each lysate were dispensed into wells of a transparent 96-well plate in triplicate. Standards of known albumin concentrations between 2 mg/mL and zero in nine levels were added to the same 96-well plate. Reagents A and B of protein kit were mixed (Pierce BCA Protein Assay Kit, Thermo Scientific, Loughborough, UK) and 200 µL were added to each well and then shaken at 400 rpm for 2 minutes. The plate was incubated in 37°C in a CO_2-free incubator for 30 minutes in a bag to prevent evaporation. The absorbance was measured in each assay well (one scan) using Spectra Max Multiple microplate reader (Molecular Devices, Wokingham, UK)

Total ATP Assay

Age-matched normal and glaucoma LC cells were seeded at a density of 10,000 cells/well (cell numbers were previously optimized for each assay to produce a measurable signal) in a total volume of 100 µL of low glucose (1000 mg/L) DMEM growth medium supplemented with L-glutamine and antibiotics in a transparent standard flat bottom 96-well plate. After 24 hours, medium was carefully removed from the LC cells and replaced with 200 µL wash per well of fresh medium (DMEM) without phenol red containing either 10 mM glucose (Sigma-Aldrich) or 10 mM galactose (Sigma-Aldrich) in addition to 2 mM L-glutamine (Sigma-Aldrich) and 1 mM sodium pyruvate (Sigma-Aldrich), and 20 mM HEPES buffer (1M, Sigma-Aldrich) was added. Next, the wash media was replaced with 100 µL per well of either glucose or galactose containing medium as before. We added 0.25 µM of carbonyl cyanide-4-trifluoromethoxyphenylhydrazone (FCCP) to certain wells as a mitochondrial uncoupler, the remaining wells received dimethyl sulfoxide (DMSO, Sigma-Aldrich) as a vehicle control in the same concentration as in FCCP-treated wells. Assays were conducted in triplicate. The plate was then incubated in a CO_2 incubator at 37°C. Three hours later, the plate was taken out and 100 µL of the reaction mixture CellTiter-Glo 2.0 assay (Promega, Dublin, Ireland) prepared as per the manufacturer's protocol was immediately added to all wells and the cells were shaken at 400 rpm for 2 minutes using a rotation shaker. The whole content of each well was transferred to a white 96-well plate (Thermo Fischer Scientific, Cork, Ireland) and the chemiluminescence signal was measured using VICTOR X4 multilabel microplate reader (PerkinElmer) after adjusting temperature to 37°C according to manufacturer's protocol (one scan).

OCR Assay

Age-matched normal and glaucoma LC cells were seeded at a density of 50,000 cells/well (cell numbers were previously optimized for each assay to produce a measurable signal) in a total volume of 100 µL of standard DMEM growth medium supplemented with L-glutamine and antibiotics in a transparent flat bottom 96-well plate for 24 hours. The next day, the medium was carefully removed and replaced with 200 µL of fresh (DMEM respiration medium) containing 10 mM glucose, 2 mM L-glutamine, 1 mM sodium pyruvate, and 20 mM HEPES (pH 7.2–7.4). The plate was incubated for 30 minutes in a CO_2 incubator at 37°C. Afterwards, the medium was replaced with 100 µL of the respiration medium containing 200 nM O_2-sensitive probe (MitoXpress–Xtra HS kit MX-200, Luxcel Biosciences). We added 0.25 µM FCCP (mitochondrial uncoupler of ATP synthesis and the electron transport chain) and 0.25 µM DMSO to the designated wells. Other wells received antimycin A (an electron transport inhibitor through binding to cytochrome C reductase) with a final concentration of 1 µM as a mitochondrial inhibitor. The assays were conducted in triplicate with other wells containing no cells as negative controls. We added 150 µL of prewarmed mineral oil (37°C) immediately to all wells to block ambient oxygen from the cells and the luminescent signal was measured every 30 seconds using a VICTOR X4 multilabel microplate reader (PerkinElmer) after adjusting temperature to 37°C according to manufacturer's protocol for at least 60 minutes. Probe phosphorescence signals are reversibly quenched of by O_2; hence, depletion of sample O_2 owing to cell respiration increases probe signals.

RNA Extraction, cDNA Synthesis, and Quantitative Real-Time RT-PCR

Total RNA was isolated from normal and glaucoma LC cells using Tri-Reagent (Life Technologies, Dublin, Ireland) as per the manufacturer's instructions. Total RNA (2 µg) was reverse transcribed into cDNA using enhanced avian reverse transcriptase (eAMV) (Sigma), oligo dT (Sigma), deoxynucleotides (dNTPs) (Sigma) and the corresponding primers.

Relative expression of the genes of interest was assessed by quantitative RT-PCR on a Rotorgene 3000 Real-Time PCR Thermocycler (Labortechnik, Wasserburg, Germany) using QuantiTect SYBR Green PCR Master Mix (Qiagen, North Manchester, Ireland). GAPDH was considered to be an internal control. The sequences of specific PCR primers (100 nM) were given as follows: MCT1: forward: 5′-TGTTAGTCGGAGCCTTCATTTC-3′; reverse: 5′-CACTGGTCGTTGCACTGAATA-3′, MCT4: forward: 5′-TCACGGGTTTCTCCTACGC-3′; reverse: 5′-GCCAAAGCGGTTCACACAC-3′, MTHFD2: forward: 5′-TACTCCATGGGGTGTGTGG-3′; reverse: 5′-GGGCATTCCAACGTTTT-3′, GLS2: forward: 5′- AGCGTATCCCTATCCACAAGTTCA-3′; reverse: 5′- GCAGTCCAGTGGCCTTCAGAG-3′, GAPDH: forward: 5′-CCATTCTTCCACCTTTGATGCT-3′; reverse: 5′-TGTTGCTGTAGCCATATTC-ATTGT-3′.

Each PCR product was analyzed based on the individual cycle threshold by the GAPDH standard curve. All gene expression levels were normalized to GAPDH, and data were quantified according to the method of Livak and Schmittgen[34] and presented as the mean ± SD of at least three LC cell samples derived from normal and glaucoma individuals.

Investigative Ophthalmology & Visual Science

Cell Lysate Preparation and Western Blot Analysis

The protein expression levels of MCT1, MCT4, GLS2. and MTHFD2 in LC cells were quantified by Western blotting. Normal and glaucoma LC cells were grown to 90% confluence in T75 tissue culture flasks, depleted of serum for 24 hours and proteins were extracted as follows. Cells were rinsed twice with ice-cold phosphate-buffered saline and collected by scraping the culture dishes with cell scrapers into ice-cold phosphate-buffered saline. Cells were centrifuged (1000×*g* for 10 minutes at 4°C) and the supernatant removed. The cells were then lysed in radio immunoprecipitation assay buffer supplemented with a protease and phosphatase inhibitor cocktail (Sigma Aldrich), incubated on ice for 5 minutes and centrifuged at 4°C at 13,000×*g* for 10 minutes to remove cell debris. The supernatant containing proteins was collected, flash frozen, and stored at −80°C until processing. Protein concentrations were measured by BCA protein assay kit (Sigma Aldrich). Equal amounts of cellular proteins (20 µg/lane) were mixed with Laemmli's sample buffer and boiled at 95°C for 5 minutes,[35] separated on 10% polyacrylamide-SDS gels and transferred to nitrocellulose membranes. Membranes were blocked with 5% nonfat milk in Tris-buffered saline containing 0.1% Tween-20 (TBST) for 1 hour and then incubated overnight at 4°C with the following primary antibodies: anti-MCT1 (Abcam 1:500), anti-MCT4 (Abcam 1:500), anti-GLS2 (Abcam 1:500), and anti-MTFHD2 (Abcam 1:500). After three washes with TBST solution, membranes were subsequently incubated for 1 hour at room temperature with either with anti-rabbit or anti-mouse IgG–horseradish peroxidase-conjugated secondary antibodies (1:5000) in TBST. Bound antibody was detected using immunoblotting according to standard protocols using the ECL detection system (Fisher Scientific, Dublin, Ireland). Membranes are reprobed with anti–β-actin antibodies as loading controls. Band size and density measurements from each sample were collected using ImageJ (National Institutes of Health, Bethesda, MD). Values were normalized by the levels of β-actin.

Statistical Analysis

Data were expressed as the mean ± SD. Groups were compared using one-way ANOVA with a post hoc test for comparison of three or more groups and with a Student two-tailed *t* test when comparing two groups; *P* values of less than .05 were taken to indicate a statistically significant difference. Calculations were performed by the Origin 7.0 software (Origin Lab, Bucks, UK).

Results

ECA

To compare the bioenergetics status of glaucoma with normal control LC cells, ECA analysis was performed first. Figure 1 shows a representative example of a corrected LT profiles for pH probe signals for an experiment of L-ECA (Fig. 1A) and T-ECA (Fig. 1B) obtained from LC cells from one normal and one glaucoma donor eye after correcting for nonspecific drift of probe signal owing to temperature and gas equilibration. These curves represent the readings before normalization to total protein content.

To convert the corrected LT readings to actual pH figures, and subsequently calculate the pH change profiles from the previous curves in Figures 1A and 1B, we used the following equation: pH = (1893.4 – LT)/227.54, according to the protocol.[36] To calculate the rate of pH change per minute for L-ECA (Fig. 1C) and T-ECA (Fig. 1D), the slopes were calculated from 0 to 40 minutes to exclude later results as the probe decays.

Data from each experiment were normalized to the total protein content of either the normal or glaucoma LC cells. Normal LC cells within 225 µL of ECA medium in one well contained 0.180 mg protein, whereas glaucoma LC cells within 225 µL of ECA medium in one well contained 0.338 mg protein (more proliferation seen in all glaucoma wells after 24 hours of seeding). After normalizing the previously mentioned representative experiment to total protein content, we found a higher L-ECA and T-ECA rate of pH change per minute in normal LC cells compared with glaucoma LC cells (Figs. 2A and 2B).

Interestingly, we found a higher contribution of L-ECA to T-ECA in glaucoma LC cells compared with normal LC cells (Fig. 2C). These results were statistically significant looking at the average of all donors. (85.97 ± 3.71% vs. 63.97 ± 9.34%, respectively; $n = 3$; $P < .05$). Taken together, these results suggest increased glycolytic flux and decreased OXPHOS in glaucoma LC cells.

ATP Levels Assay

When we examined the average results of all donors and set glucose + DMSO (baseline levels) for all normal LC cells at 100 a.u., we found a statistically significant difference between normal and glaucoma LC cells in basal ATP levels (100 a.u. vs. 85.99 ± 1.73 a.u. respectively, $n = 3$; $P < .001$); we then found a larger difference when glucose was replaced with galactose (108.38 ± 17.55 a.u. [normal] vs. 84.56 ± 7.58 a.u. [glaucoma]; $n = 3$; $P < .04$). In concordance with ECA data, this result indicates mitochondrial dysfunction in glaucoma LC cells (Fig. 3).

We found that glaucoma LC cells produce less basal levels of ATP compared with normal LC cells, when glucose is used with DMSO as a vehicle control after normalization to total protein content. The difference between normal and glaucoma increases when the mitochondria are stressed by using galactose instead of glucose, because galactose cannot be used by glycolysis which forces the cells to rely more on OXPHOS to produce ATP.

Interestingly, when supplied with glucose but uncoupled with FCCP, cells showed comparable ATP levels; in other words, the relative decrease in ATP levels is smaller in glaucoma cells. This outcome could be due to the fact that, upon uncoupling, F1F0-ATP synthase (i.e., complex V of the electron transport chain) reverses its activity and becomes one of the major consumers of glycolytic ATP.[37] Glaucoma cells seem to cope better with this stress because glycolytic flux provides cells with greater amounts of ATP.

In this set of experiments, galactose was used instead of glucose with FCCP as a negative control, because ATP production is inhibited through both glycolysis and OXPHOS. Treatment of LC cells with FCCP resulted in a significant reduction of ATP production levels when FCCP is added to the cells deprived of glucose (Fig. 3).

The ATP assay shows decreased basal ATP levels in glaucomatous LC cells compared with normal cells. This finding may suggest decreased overall metabolic activity and ATP

Investigative Ophthalmology & Visual Science

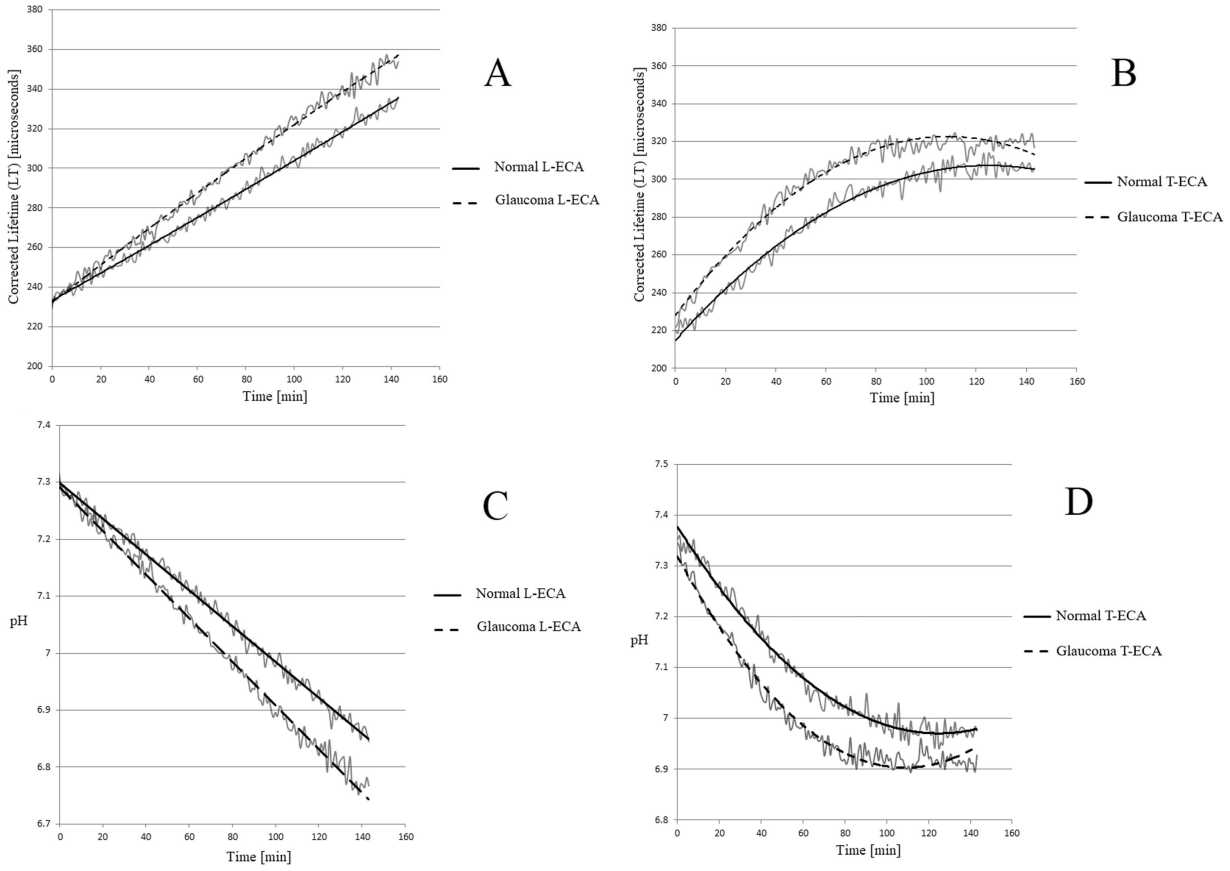

Figure 1. Lactate-related (L) and Total (T) ECA measurements and corresponding pH profiles in LC cells (representative examples) (**A**) Representative example of a corrected LT profile for pH probe signal from a L-ECA experiment of one normal and one glaucoma LC cell donor. (**B**) Corrected LT profiles for pH probe signal from a T-ECA experiment of one normal and one glaucoma LC cell donor. These curves represent the readings before normalization to total protein content, and they are corrected for nonspecific drift of probe signal owing to temperature and gas equilibration. (**C**) Corresponding pH profiles of (**A**). (**D**) Corresponding pH profiles of (**B**). (Each curve represents an average of triplicate.) To calculate the pH change profiles from the previous curves in (**A**) and (**B**), the following equation was used (pH = [1893.4 – LT]/227.54).

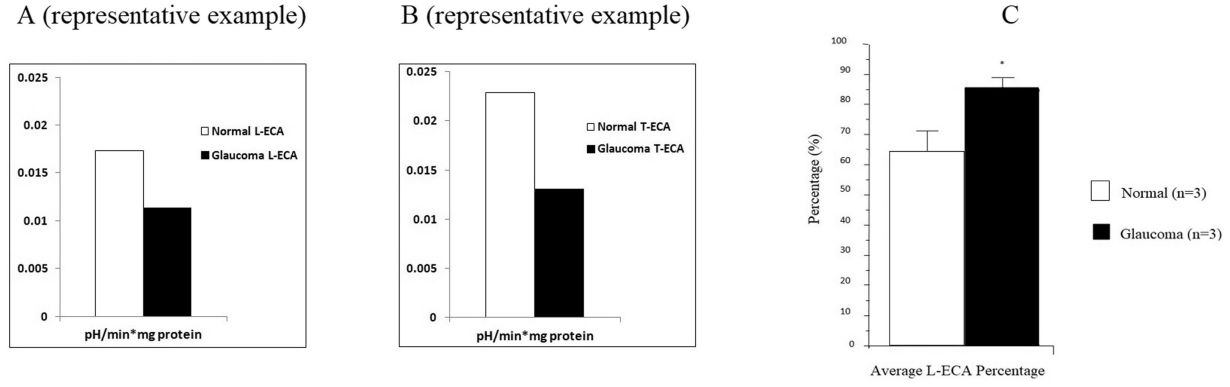

Figure 2. ECA data normalized to total protein content and average lactic acid contribution to the T-ECA. Normalized (**A**) L-ECA and (**B**) T-ECA results from a representative experiment on one normal and one glaucoma LC cell donor (average of triplicate) calculated from Figures 1C and 1D. To calculate the rate of pH change per minute, the slopes were calculated from 0–40 minutes to exclude later results as the probe decays. (**C**) The higher contribution of L-ECA to T-ECA in glaucoma LC cells compared with normal LC cells. These results were statistically significant looking at the average of all donors (85.97 ± 3.71% vs. 63.97 ± 9.34%, respectively; $n = 3$; $P < .05$). This indicates an increase in aerobic glycolysis and a decrease in OXPHOS in glaucoma LC cells. Error bars = standard deviation. * $P < .05$.

fluxes, whether it is glycolysis or OXPHOS. In the previous ECA assay (Fig. 2), T-ECA rates reflect combined rates of lactate production and CO_2 release, with the latter being contributed mainly by the Krebs cycle and pentose phosphate pathway. Although both L-ECA and T-ECA rates in glaucoma cells are lower than in control (Figs. 2A and 2B),

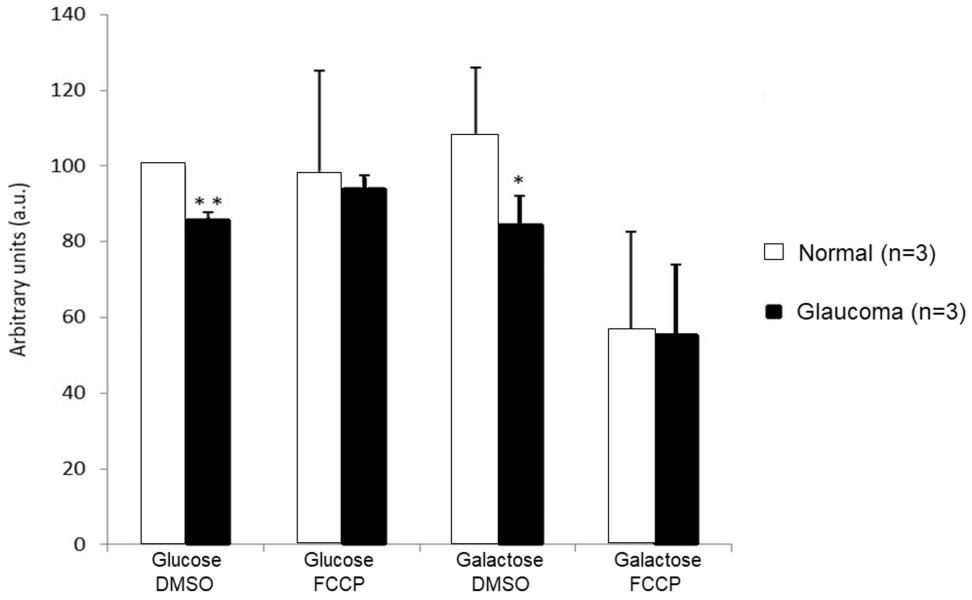

Figure 3. ATP levels measured in normal and glaucoma LC cells. Average normalized ATP levels from all donors of normal and glaucoma LC cells. Glucose + DMSO (baseline levels) for all normal LC cells set at 100 a.u. Results show a statistically significant difference between normal and glaucoma LC cells in basal ATP levels (100 a.u. vs. 85.99 ± 1.73 a.u. respectively; $n = 3$; $P < .001$); with a greater difference when galactose was used instead of glucose—to stress the mitochondria—(108.38 ± 17.55 a.u. [normal] vs. 84.56 ± 7.58 a.u. [glaucoma]; $n = 3$; $P < .04$). This finding is indicative of mitochondrial dysfunction in glaucoma LC cells. DMSO, dimethyl sulfoxide; FCCP, carbonyl cyanide-4-trifluoromethoxyphenyl-hydrazone. Error bars = standard deviation. *$P < .04$. ** $P < .001$.

the increased L-ECA/T-ECA ratio shows that in diseased state (i.e., glaucoma) glycolysis is more active relative to the Krebs cycle and, consequently, to OXPHOS.

OCR

Figure 4A shows a representative example of corrected LT profiles for O_2 probe signals for a typical OCR experiment. These data are from one donor of normal and glaucoma LC cells after correcting for nonspecific drift of probe signal owing to temperature and gas equilibration. These curves include basal respiration (DMSO), with FCCP (uncoupler) to measure mitochondrial respiratory spare capacity or with antimycin A (mitochondrial inhibitor) as a negative control. Note that all these curves are plotted before normalization to total protein content.

Next, to calculate the O_2 concentration profiles, we used the following equation (where e is an exponential function) according to the protocol[36] as shown in Figure 4B.

$$[O_2] = 4,455.46 \times e^{-LT/7.48284}$$

Then, to calculate the OCR per minute, the slopes were calculated from 0 to 40 minutes to exclude later points owing to probe decay.

To be able to obtain representative results, all OCR data had to be normalized to the total protein content of the corresponding normal or glaucoma LC cells. The average of all donors showed a lower basal OCR in glaucoma LC cells compared with that in normal control LC cells (1.99 ± 0.80 vs. 7.73 ± 1.9 nM/min*mg protein, respectively; $n = 3$; $P < .001$). Also, there was a diminished spare capacity of OCR in glaucoma LC cells compared with normal LC cells (4.94 ± 0.6 vs. 13.28 ± 1.28 nM/min*mg protein, respectively; $n = 3$; $P < .001$), as shown in Figure 4C. These results indicate lower basal mitochondrial respiration and decreased respiratory spare capacity in glaucoma LC cells compared with normal LC cells.

Alternative Energy Pathways

To assess the potential significance of MCT1, MCT4, MTHFD2, and GLS2 in normal and glaucoma LC cells, we first examined whether there was differential expression levels of their mRNA using quantitative real-time RT-PCR. As illustrated in Figure 5A (*$P < .05$, ** $P < .02$), MCT1, MCT4, MTHFD2, and GLS2 transcription was detected at low levels from the average data of three normal LC cell donors, but significantly upregulated taking the average of three glaucoma LC cell donors. These results clearly showed that mRNA transcription levels were significantly enhanced in glaucoma LC cells.

Having shown that the *MCT1*, *MCT4*, *MTHFD2*, and *GLS2* genes are differentially expressed in normal and glaucoma LC cells, we were prompted to further assess their protein expression. In accordance to gene expression analysis, a representative experiment of western blotting analysis showed that the protein expression levels of MCT1, MCT4, MTHFD2, and GLS2 are higher in glaucoma LC cell donor compared with the normal LC cell donor (Fig. 5B). Average data illustrating the protein expression of MCT1, MCT4, MTHFD2, and GLS2 in LC cell lines obtained from three normal donors and three glaucoma individuals showed significantly elevated protein expression levels in glaucoma LC cells (Fig. 5C) (*$P < .05$).

Discussion

The present study shows evidence of bioenergetic mitochondrial respiratory dysfunction in human

Investigative Ophthalmology & Visual Science

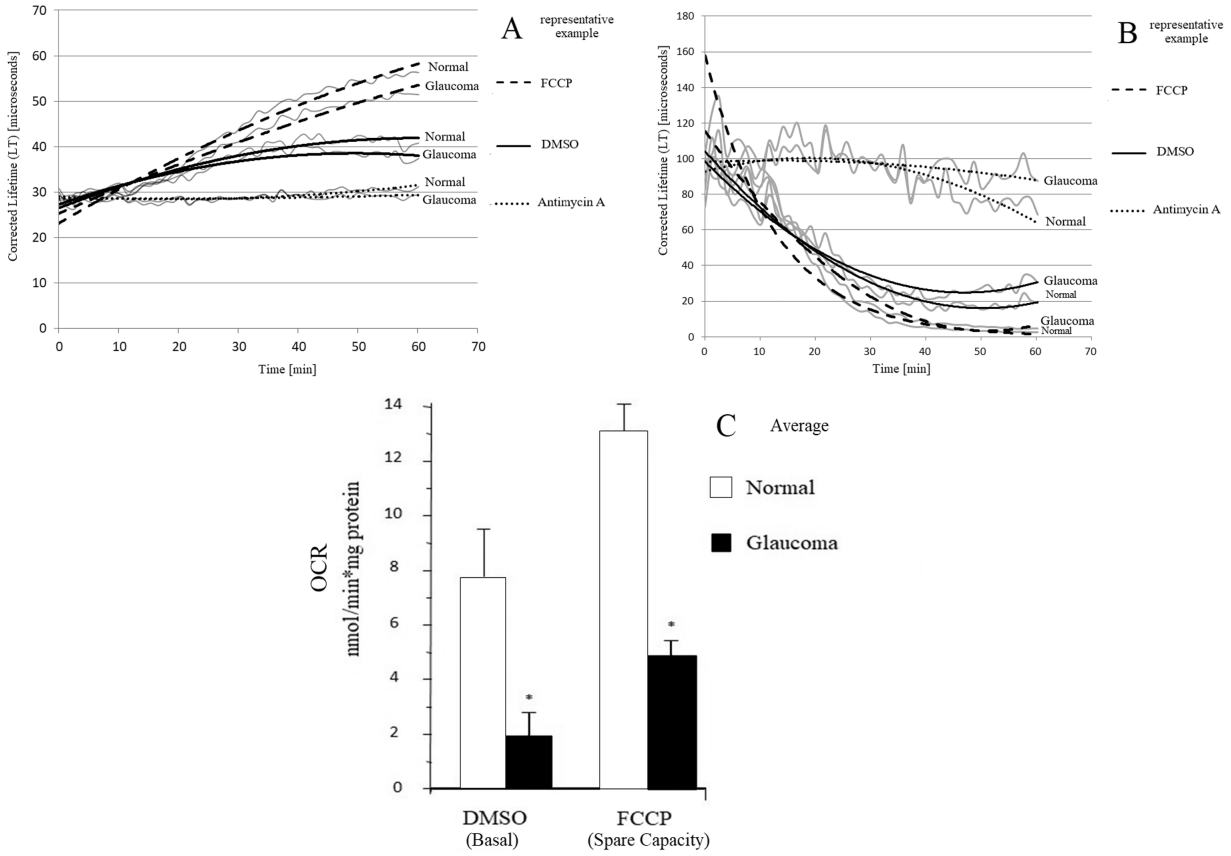

Figure 4. OCR measurement in LC cells (before and after normalization to total protein content). (**A**) Corrected LT profiles for O_2 probe signal from a representative example of an OCR experiment of one donor of normal and glaucoma LC cells (average of triplicate). DMSO used as a vehicle control for basal respiration. FCCP was used to measure mitochondrial respiratory spare capacity. Antimycin A was used as a negative control. (**B**) Corresponding O_2 concentration profiles of (**A**). These curves represent the readings before normalization to total protein content, and they are corrected for nonspecific drift of probe signal owing to temperature and gas equilibration. (**C**) Average data of basal OCR (DMSO) and spare capacity of OCR (FCCP) from all donors (each in triplicate). To calculate the OCR per minute, the slopes from (B) were calculated from 0 to 40 minutes to exclude later results with probe decay. To be able to obtain representative results, all figures had to be normalized to the total protein content of the corresponding normal or glaucoma LC cells. The average of all donors showed a decrease in basal OCR in glaucoma LC cells compared with normal LC cells (1.99 ± 0.80 vs. 7.73 ± 1.9 nM/min*mg protein, respectively; $n = 3$; $P < .001$). Also there was a diminished spare capacity of OCR in glaucoma LC cells compared with normal LC cells (4.94 ± 0.6 vs. 13.28 ± 1.28 nM/min*mg protein respectively, $n = 3$; $P < .001$). These results indicate decreased basal OXPHOS and decreased mitochondrial respiratory spare capacity in glaucoma LC cells compared with normal LC cells. Error bars = standard deviation. * $P < .001$.

glaucomatous LC cells as evidenced by reduced ATP production, reduced OXPHOS, and increased lactate contribution in ECA compared with normal control LC cells. We also measured markers of OXPHOS, glycolysis, the folate-mediated one-carbon metabolism and glutaminolysis, and found that glaucoma LC cells display significantly enhanced transcription and expression levels of MCT1, MCT4, MTHFD2, and GLS2, respectively.

We showed that glaucoma LC cells produced significantly less ATP at basal levels compared with normal control LC cells, and the gap widens when mitochondrial OXPHOS capacity to produce ATP is assessed by forcing the cells to use galactose only (Fig. 3). This finding, together with increased glycolysis and reduced OXHPOS in glaucoma LC cells (Figs. 2 and 4), suggests an effect similar to the Warburg effect described in cancer cells.[38] Although glaucoma LC cells have a decreased spare capacity of OCR compared with normal LC cells (Fig. 4C), they are able to produce an equivalent amount of ATP as normal LC cells when ATP production from OXHPOS is uncoupled with FCCP (Fig. 3). This result is probably attributed to the increased capacity of glaucoma LC cells to rely on glycolysis for their ATP requirements. This is another major support of the suggested Warburg effect in glaucoma LC cells.

Otto Warburg described how cancer cells are prone to aerobic glycolysis rather than aerobic oxidation of substrates by mitochondria, a phenomenon termed the Warburg effect.[39] The role of the Warburg effect may go far beyond energy production, because the metabolites generated by aerobic glycolysis participate in the regulation of different cellular functions, including proliferation, autophagy, apoptosis, and ECM production.[40] An example of altered OXPHOS has been found in cancer cells; this alteration may lead to loss of enzyme function with subsequent stabilization of hypoxia-inducible factor 1α, an important component of the oxygen-sensing pathway. Hypoxia-inducible factor 1α is a transcription factor that, when stabilized, becomes translocated into the nucleus and causes a shift in energy metabolism from oxidative to glycolytic states.[41] A recent study found that lung fibroblasts of interstitial pulmonary fibrosis have a reduced ATP content and a reduced rate of OCR indicating poor mitochondrial function.[42] It has

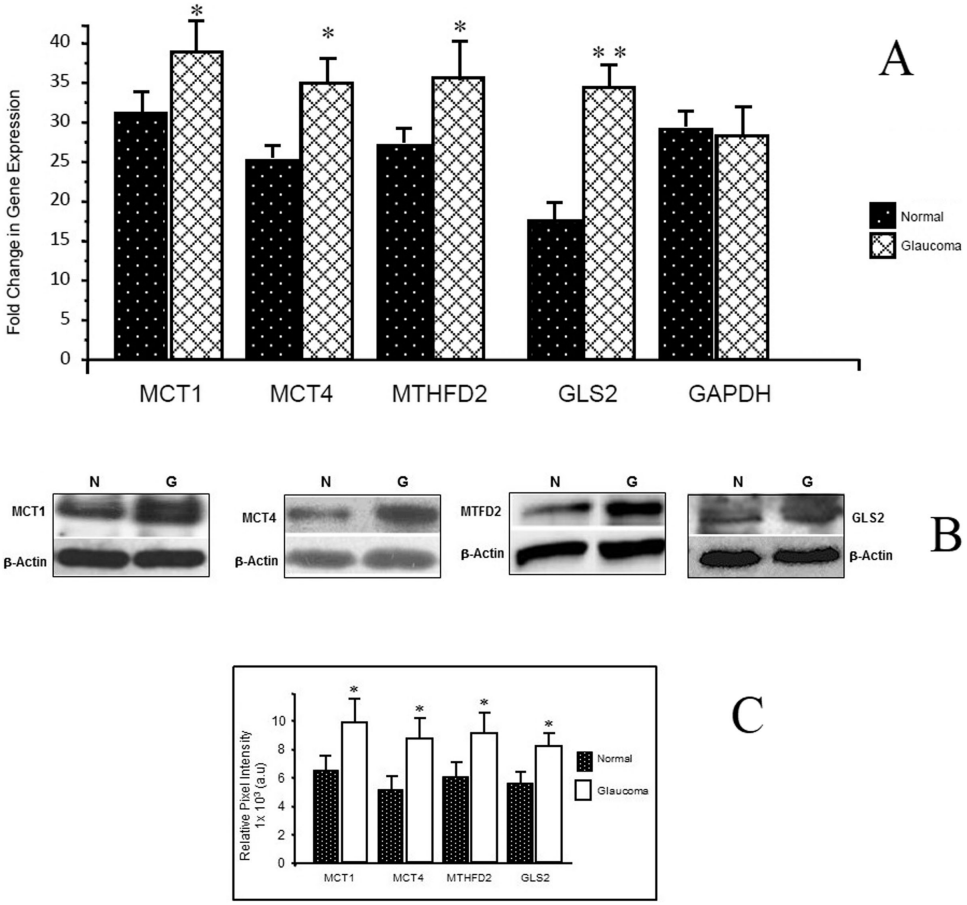

Figure 5. mRNA and protein expression of MCT1, MCT4, MTHFD2, and GLS2 in normal and glaucoma LC cells. (**A**) Average data of quantitative real time RT-PCR comparing the transcription levels of MCT1, MCT4, MTHFD2, and GLS2 in LC cells obtained from three normal controls and three glaucoma LC cell donors. Note that MCT1, MCT4, MTHFD2, and GLS2 transcription levels are all significantly upregulated in glaucoma LC cells relative to normal control LC cells. GAPDH was used as an internal control, with the same level of expression seen in both normal and glaucoma LC cells. (**B**) Representative experiment of protein expression of MCT1, MCT4, MTHFD2, and GLS2 was performed by western immunoblotting in normal (N) and glaucoma (G) LC cells. β-Actin was used as a loading control, with the same level of expression seen in normal and glaucoma cell lysates. (**C**) Average data illustrating the protein expression of MCT1, MCT4, MTHFD2, and GLS2 in LC cell lines obtained from three normal control donors and three patients with glaucoma. Western blots using specific anti- MCT1, MCT4, MTHFD2, and GLS2 antibodies revealed MCT1, MCT4, MTHFD2, and GLS2 are expressed at lower levels in normal LC cells; however, their expression level was enhanced in glaucoma LC cells (two-tailed unpaired Student *t* test). Results are expressed as relative pixel intensity versus normal control LC cell samples. Error bars = standard deviation. * $P < .05$. ** $P < .02$.

been also reported that mitochondrial dysfunction in interstitial pulmonary fibrosis lung cells contributes to maladaptation to cellular stress and promotes the development of pulmonary fibrosis.[11] Laryngotracheal stenosis is a chronic fibrotic disease characterized by fibroblast proliferation and matrix remodeling in the lamina propria of the larynx and trachea. A recent study using fibroblasts from both normal controls and patients with laryngotracheal stenosis found a higher proliferation rate in laryngotracheal stenosis fibroblasts. Furthermore, a cellular metabolic analysis in these cells revealed reduced OXPHOS and increased glycolysis compared with normal fibroblasts.[12]

Another example of cell bioenergetics alteration is seen in cancer-associated fibroblasts. These fibroblasts supply adjacent cancer cells with anapleurotic substrates, such as lactate derived from their own excessive glycolysis. They thereby induce OXPHOS in the adjacent cancer cells, allowing them to produce large amounts of ATP necessary for their proliferation.[43] Metabolic reprogramming of fibroblasts into a cancer-associated fibroblast phenotype is mediated by high amounts of hydrogen peroxide (H_2O_2) generated by cancer cells, which creates a pseudohypoxic state mimicking oxygen and nutrient depletion.[44] The lack of fuel for OXPHOS results in lower ATP output and increased AMP/ATP ratio which activates adenosine monophosphate-activated protein kinase (AMPK) and results in activation of glycolysis through (a) the phosphorylation of phosphofructokinase 2 and (b) elevated glucose uptake by means of glucose transporter type 4 expression.[45] This model of cell bioenergetic alteration may suggest that our findings of glaucomatous LC cells metabolic abnormality is secondary to a chronic insult originating from the well-established oxidative stress in glaucomatous eyes, in addition to the mechanical stress imposed by an increased IOP, rather than a primary inherent malfunction of these cells.

Mitochondrial dysfunction has been previously investigated at different levels in glaucoma patients.[46] These include defective mitochondrial function in trabecular

Investigative Ophthalmology & Visual Science

meshwork cells of POAG patients with subsequent failure of IOP control.[47] In addition, AMPK was identified as a critical regulator of ECM homeostasis and cytoskeletal arrangement in primary cultured human trabecular meshwork cells, with mice that are AMPKα2-null showing higher IOPs and decreased aqueous clearance compared with their wild-type counterparts.[48] Another recent study on DBA/2J mouse models demonstrated that the AMPK activation apparent in the glaucomatous retina and optic nerve triggers NF-κB signaling which induces a proinflammatory response. A ketogenic diet has a neuroprotective effect by ameliorating this inflammation by inhibition of AMPK activation.[49] Analysis of ATP production and complex I–linked respiration in human lymphoblasts has been used to characterize mitochondrial dysfunction in patients with POAG.[50] Also, a recent study compared the degree of OXPHOS impairment in POAG and Leber's hereditary optic neuropathy lymphoblasts to test whether the milder clinical disease in POAG correlated with a milder complex I impairment. To assess overall mitochondrial capacity, cells were required to produce ATP primarily from galactose. This study showed that complex I activity in lymphoblasts was less impaired in POAG compared with Leber's hereditary optic neuropathy, which might reflect the less aggressive progression of disease in POAG.[51] A study by Lascaratos et al.[52] showed healthier mitochondria in ocular hypertension subjects at a systemic level compared with lymphocytes from normal tension glaucoma patients and normal controls. A recent study has also assessed the contribution of mitochondrial genetic variation to POAG pathogenesis using Gene-Set analyses, suggesting the importance of lipid and carbohydrate metabolism in the disease process.[53]

Mitochondrial dysfunction also has been implicated in RGC loss in animal models of glaucoma,[54] whereas nicotinamide has shown to be neuroprotective against glaucoma in DBA/2J mice, including its prevention of optic nerve excavation and axon loss as assessed by histologic analysis and axon counting.[55] Mitochondrial dysfunction promotes the susceptibility of RGC, which has high energy requirements, to stress from other risk factors, including increased IOP and vascular insufficiency.[56] Optic nerve axonal injury in Thy1-UFPH mice triggered upregulation of the stress-induced protein REDD2 (regulated in development and DNA damage response 2), a potent inhibitor on mammalian target of rapamycin. Subsequently, this promoted dendrite pathology causing neuronal dysfunction and cell death.[57] In contrast, human recombinant insulin, administered as eye drops or systemically after dendritic arbor shrinkage in RGCs and before cell death, promoted robust regeneration of dendrites and synapses with successful circuit function restoration.[58] Furthermore, the PI3K/Akt pathway has been shown to play a crucial role in RGC protection against glaucomatous injury.[59]

Our study showed that there is increased glycolysis in glaucomatous LC cells. To alleviate cells from pH stress owing to acidification, the MCT family members, particularly the proton symporters MCT1 and MCT4, are highly activated, regulate the uptake and release of lactate from fibrotic and cancer cells, adapt these cells to acidification, and stabilize the tissue microenvironment. This is done in coordination with the folate-mediated one-carbon enzyme MTHFD2 and GLS2. Therefore, MCT1, MCT4, MTHFD2, and GLS2 are key players in maintaining the hyperglycolytic and acid-resistant phenotypes of cells in fast growing tissues. We found that glaucoma LC cells show higher transcription and expression levels of MCT1, MCT4, MTHFD2, and GLS2.

The major physiologic roles of MCT1 and MCT4 are to regulate cellular lactic acid transport, depending on their metabolic state. During hypoxia, cells become more dependent on glycolysis for their ATP production and consequently require export of lactic acid which is mediated by MCT1, which is the major expressed isoform in most tissues.[60] MCT4 is more specifically expressed in tissues that depend on glycolysis.[60,61] MCT4 expression has also been found to be upregulated in the central hypoxic-zone fibroblasts of keloids, which is a fibro-proliferative skin disorder with tumor-like behavior and dependence on aerobic glycolysis.[16] In addition, MCT1 and MCT4 have been shown to colocalize with Emmprin (Basigin, CD147),[62] which is a cell surface glycoprotein that induces ECM metalloproteinase. Our group has previously demonstrated increased expression of Emmprin by immunohistochemistry in human POAG optic nerve head tissue compared with nonglaucomatous controls.[63] MCT1 and MCT4 inhibitors can prevent further lactic acid production and block cell proliferation by acting as potent immunosuppressant drugs.[64]

Dietary folate is an essential requirement for fast proliferating cells through nucleic acid synthesis. Overexpression of mitochondrial enzyme MTHFD2 is associated with elevated cell proliferation rates.[65] MTHFD2 is a key player in folate-dependent carbon metabolism, and therefore represents a powerful target for the inhibition of rapidly replicating cells. These enzymes are targeted by drugs such as methotrexate.[66] MTHFD2 is highly overexpressed in cancer tissues and embryonic cells, but not in normal adult tissues. The development of inhibitors targeting MTHFD2,[67] is an attractive opportunity to specifically target proliferating cells such as cancer and probably glaucoma LC cells.

Increased glutamine metabolism (glutaminolysis) has been recognized as a key metabolic change in cancer cells, along with increased aerobic glycolysis (the Warburg effect).[68] GLS is an enzyme that generates glutamate from glutamine. Two genes encode GLSs in human cells: GLS1 (also known as kidney-type GLS), and GLS2 (also known as liver-type GLS). GLS2 is transcriptionally upregulated by the tumor suppressor p53 and mediates p53's regulation of mitochondrial function and antioxidant defense in cells.[69] Ectopic expression of GLS2 greatly inhibited the growth and colony formation of human hepatocellular carcinoma cells in vitro and the growth of xenograft tumors in vivo.[69,70] GLS inhibitors may play a role in suppressing tumor growth and proliferation.[71]

There is a clear unmet clinical need to develop novel treatments to halt the progressive and ongoing fibrotic damage to the LC in glaucomatous optic nerves. Here, we expanded further on mitochondrial function of these distinct type of cells in human glaucoma patients by performing a detailed bioenergetic assessment (ATP, OCR, and ECA) in normal nonglaucomatous and glaucomatous human individuals, which revealed further evidence of mitochondrial dysfunction. In contrast, the markers of mitochondrial metabolism assessed here, MCT1/4, MTHFD2, and GLS2 are upregulated in glaucoma LC cells relative to normal controls. Therefore, future research will determine whether these compounds are viable therapeutic targets.

Investigative Ophthalmology & Visual Science

Acknowledgments

Cofunded by the Irish College of Ophthalmologists/Novartis Research Award 2015/2016 and the International Glaucoma Association/Royal College of Ophthalmologists Grant 2017.

Disclosure: **K. Kamel,** None; **C.J. O'Brien,** None; **A.V. Zhdanov,** None; **D.B. Papkovsky,** None; **A.F. Clark,** None; **D. Stamer,** None; **M. Irnaten,** None

References

1. Quigley HA, Broman AT. The number of people with glaucoma worldwide in 2010 and 2020. *Br J Ophthalmol*. 2006;90(3):262–267.
2. Yang H, Reynaud J, Lockwood H, et al. The connective tissue phenotype of glaucomatous cupping in the monkey eye - clinical and research implications. *Prog Retin Eye Res*. 2017;59:1–52.
3. Danford ID, Verkuil LD, Choi DJ, et al. Characterizing the "POAGome": a bioinformatics-driven approach to primary open-angle glaucoma. *Prog Retin Eye Res*. 2017;58:89–114.
4. Quigley HA, Hohman RM, Addicks EM, Massof RW, Green WR. Morphologic changes in the lamina cribrosa correlated with neural loss in open-angle glaucoma. *Am J Ophthalmol*. 1983;95(5):673–991.
5. Hernandez MR, Andrzejewska WM, Neufeld AH, Changes in the extracellular matrix of the human optic nerve head in primary open-angle glaucoma. *Am J Ophthalmol*. 1990;109(2):180–188.
6. Hartman R, Patil P, Tisherman R, et al. Age-dependent changes in intervertebral disc cell mitochondria and bioenergetics. *Eur Cell Mater*. 2018;36:171–183.
7. Riwanto M, Kapoor S, Rodriguez D, Edenhofer I, Segerer S, Wüthrich RP. Inhibition of aerobic glycolysis attenuates disease progression in polycystic kidney disease. *PLoS One*. 2016;11(1):e0146654.
8. Kottmann RM, Kulkarni AA, Smolnycki KA, et al. Lactic acid is elevated in idiopathic pulmonary fibrosis and induces myofibroblast differentiation via pH-dependent activation of transforming growth factor-beta. *Am J Respir Crit Care Med*. 2012;186(8):740–751.
9. Fiaschi T, Marini A, Giannoni E, et al. Reciprocal metabolic reprogramming through lactate shuttle coordinately influences tumor-stroma interplay. *Cancer Res*. 2012;72(19):5130–5140.
10. Soubannier V, McBride HM. Positioning mitochondrial plasticity within cellular signaling cascades. *Biochim Biophys Acta*. 2009;1793(1):154–170.
11. Mora AL, Bueno M, Rojas M. Mitochondria in the spotlight of aging and idiopathic pulmonary fibrosis. *J Clin Invest*. 2017;127(2):405–414.
12. Ma G, Samad I, Motz K, et al. Metabolic variations in normal and fibrotic human laryngotracheal-derived fibroblasts: a Warburg-like effect. *Laryngoscope*. 2017;127(3):E107–E113.
13. Pierre K, Pellerin L. Monocarboxylate transporters in the central nervous system: distribution, regulation and function. *J Neurochem*. 2005;94(1):1–14.
14. de Araujo GG, Gobatto CA, de Barros Manchado-Gobatto F, et al. MCT1 and MCT4 kinetic of mRNA expression in different tissues after aerobic exercise at maximal lactate steady state workload. *Physiol Res*. 2015;64(4):513–522.
15. Bovenzi CD, Hamilton J, Tassone P, et al. Prognostic indications of elevated MCT4 and CD147 across cancer types: a meta-analysis. *Biomed Res Int*. 2015;2015:242437.
16. Okuno R, Ito Y, Eid N, et al. Upregulation of autophagy and glycolysis markers in keloid hypoxic-zone fibroblasts: morphological characteristics and implications. *Histol Histopathol*. 2018;33(10):1075–1087.
17. Christensen KE, Mackenzie RE, Mitochondrial methylenetetrahydrofolate dehydrogenase, methenyltetrahydrofolate cyclohydrolase, and formyltetrahydrofolate synthetases. *Vitam Horm*. 2008;79:393–410.
18. Selcuklu SD, Donoghue MT, Rehmet K, et al. MicroRNA-9 inhibition of cell proliferation and identification of novel miR-9 targets by transcriptome profiling in breast cancer cells. *J Biol Chem*. 2012;287(35):29516–29528.
19. Curthoys NP, Watford M, Regulation of glutaminase activity and glutamine metabolism. *Annu Rev Nutr*. 1995;15:133–159.
20. Tsai HW, Motz KM, Ding D, et al. Inhibition of glutaminase to reverse fibrosis in iatrogenic laryngotracheal stenosis. *Laryngoscope*. 2020 Jan 6 [Epub ahead of print].
21. Kamel K, Farrell M, O'Brien C, Mitochondrial dysfunction in ocular disease: focus on glaucoma. *Mitochondrion*. 2017;35:44–53.
22. Zhavoronkov A, Izumchenko E, Kanherkar RR, et al. Profibrotic pathway activation in trabecular meshwork and lamina cribrosa is the main driving force of glaucoma. *Cell Cycle*. 2016;15(12):1643–1652.
23. Kirwan RP, Wordinger RJ, Clark AF, O'Brien CJ. Differential global and extra-cellular matrix focused gene expression patterns between normal and glaucomatous human lamina cribrosa cells. *Mol Vis*. 2009;15:76–88.
24. Irnaten M, Zhdanov A, Brennan D, et al. Activation of the NFAT-calcium signaling pathway in human lamina cribrosa cells in glaucoma. *Invest Ophthalmol Vis Sci*. 2018;59(2):831–842.
25. McElnea EM, Hughes E, McGoldrick A, et al. Lipofuscin accumulation and autophagy in glaucomatous human lamina cribrosa cells. *BMC Ophthalmol*. 2014;14:153.
26. McElnea EM, Quill B, Docherty NG, et al. Oxidative stress, mitochondrial dysfunction and calcium overload in human lamina cribrosa cells from glaucoma donors. *Mol Vis*. 2011;17:1182–1191.
27. Dranka BP, Benavides GA, Diers AR, et al. Assessing bioenergetic function in response to oxidative stress by metabolic profiling. *Free Radic Biol Med*. 2011;51(9):1621–1635.
28. Hill BG, Benavides GA, Lancaster JR, Jr, et al. Integration of cellular bioenergetics with mitochondrial quality control and autophagy. *Biol Chem*. 2012;393(12):1485–1512.
29. Lambert W, Agarwal R, Howe W, Clark AF, Wordinger RJ. Neurotrophin and neurotrophin receptor expression by cells of the human lamina cribrosa. *Invest Ophthalmol Vis Sci*. 2001;42(10):2315–2323.
30. Irnaten M, O'Malley G, Clark AF, O'Brien CJ. Transient receptor potential channels TRPC1/TRPC6 regulate lamina cribrosa cell extracellular matrix gene transcription and proliferation. *Exp Eye Res*. 2020;193:107980.
31. Favre C, Zhdanov A, Leahy M, Papkovsky D, O'Connor R. Mitochondrial pyrimidine nucleotide carrier (PNC1) regulates mitochondrial biogenesis and the invasive phenotype of cancer cells. *Oncogene*. 2010;29(27):3964–3976.
32. O'Flaherty L, Adam J, Heather LC, et al. Dysregulation of hypoxia pathways in fumarate hydratase-deficient cells is independent of defective mitochondrial metabolism. *Hum Mol Genet*. 2010;19(19):3844–3851.
33. Zhdanov AV, Dmitriev RI, Papkovsky DB. Bafilomycin A1 activates HIF-dependent signalling in human colon cancer cells via mitochondrial uncoupling. *Biosci Rep*. 2012;32(6):587–595.
34. Livak KJ, Schmittgen TD. Analysis of relative gene expression data using real-time quantitative PCR and the 2(-Delta Delta C(T)) method. *Methods*. 2001;25(4):402–408.

35. Laemmli UK, Cleavage of structural proteins during the assembly of the head of bacteriophage T4. *Nature*. 1970;227(5259):680–685.
36. Papkovsky DB, Zhdanov AV. Cell energy budget platform for assessment of cell metabolism. *Methods Mol Biol*. 2015;1265:333–348.
37. Zhdanov AV, Andreev DE, Baranov PV, Papkovsky DB. Low energy costs of F1Fo ATP synthase reversal in colon carcinoma cells deficient in mitochondrial complex IV. *Free Radic Biol Med*. 2017;106:184–195.
38. Warburg O, On respiratory impairment in cancer cells. *Science*. 1956;124(3215):269–270.
39. Warburg O, Wind F, Negelein E. The metabolism of tumors in the body. *J Gen Physiol*. 1927;8(6):519–530.
40. Lunt SY, Vander Heiden MG, Aerobic glycolysis: meeting the metabolic requirements of cell proliferation. *Annu Rev Cell Dev Biol*. 2011;27:441–464.
41. Wallace DC, Fan W, Procaccio V. Mitochondrial energetics and therapeutics. *Annu Rev Pathol*. 2010;5:297–348.
42. Alvarez D, Cárdenes N, Sellarés J, et al. IPF lung fibroblasts have a senescent phenotype. *Am J Physiol Lung Cell Mol Physiol*. 2017;313(6):L1164–L1173.
43. Pavlides S, Whitaker-Menezes D, Castello-Cros R, et al. The reverse Warburg effect: aerobic glycolysis in cancer associated fibroblasts and the tumor stroma. *Cell Cycle*. 2009;8(23):3984–4001.
44. Martinez-Outschoorn UE, Lin Z, Trimmer C, et al. Cancer cells metabolically "fertilize" the tumor microenvironment with hydrogen peroxide, driving the Warburg effect: implications for PET imaging of human tumors. *Cell Cycle*. 2011;10(15):2504–2520.
45. Kim J, Kundu M, Viollet B, Guan KL. AMPK and mTOR regulate autophagy through direct phosphorylation of Ulk1. *Nat Cell Biol*. 2011;13(2):132–141.
46. Lee S, Van Bergen NJ, Kong GY, et al. Mitochondrial dysfunction in glaucoma and emerging bioenergetic therapies. *Exp Eye Res*. 2011;93(2):204–212.
47. He Y, Ge J, Tombran-Tink J, Mitochondrial defects and dysfunction in calcium regulation in glaucomatous trabecular meshwork cells. *Invest Ophthalmol Vis Sci*. 2008;49(11):4912–4922.
48. Chatterjee A, Villarreal G, Jr, Oh DJ, Kang MH, Rhee DJ. AMP-activated protein kinase regulates intraocular pressure, extracellular matrix, and cytoskeleton in trabecular meshwork. *Invest Ophthalmol Vis Sci*. 2014;55(5):3127–3139.
49. Harun-Or-Rashid M, Inman DM, Reduced AMPK activation and increased HCAR activation drive anti-inflammatory response and neuroprotection in glaucoma. *J Neuroinflammation*. 2018;15(1):313.
50. Lee S, Sheck L, Crowston JG, et al. Impaired complex-I-linked respiration and ATP synthesis in primary open-angle glaucoma patient lymphoblasts. *Invest Ophthalmol Vis Sci*. 2012;53(4):2431–2437.
51. Van Bergen NJ, Crowston JG, Craig JE, et al. Measurement of systemic mitochondrial function in advanced primary open-angle glaucoma and Leber hereditary optic neuropathy. *PLoS One*. 2015;10(10):e0140919.
52. Lascaratos G, Chau KY, Zhu H, et al. Resistance to the most common optic neuropathy is associated with systemic mitochondrial efficiency. *Neurobiol Dis*. 2015;82:78–85.
53. Khawaja AP, Cooke Bailey JN, Kang JH, et al. Assessing the association of mitochondrial genetic variation with primary open-angle glaucoma using Gene-Set analyses. *Invest Ophthalmol Vis Sci*. 2016;57(11):5046–5052.
54. Ju WK, Kim KY, Angert M, et al. Memantine blocks mitochondrial OPA1 and cytochrome c release and subsequent apoptotic cell death in glaucomatous retina. *Invest Ophthalmol Vis Sci*. 2009;50(2):707–716.
55. Williams PA, Harder JM, Cardozo BH, Foxworth NE, John SWM. Nicotinamide treatment robustly protects from inherited mouse glaucoma. *Commun Integr Biol*. 2018;11(1):e1356956.
56. Kong GY, Van Bergen NJ, Trounce IA, Crowston JG. Mitochondrial dysfunction and glaucoma. *J Glaucoma*. 2009;18(2):93–100.
57. Morquette B, Morquette P, Agostinone J, et al. REDD2-mediated inhibition of mTOR promotes dendrite retraction induced by axonal injury. *Cell Death Differ*. 2015;22(4):612–625.
58. Agostinone J, Alarcon-Martinez L, Gamlin C, Yu WQ, Wong ROL, Di Polo A. Insulin signalling promotes dendrite and synapse regeneration and restores circuit function after axonal injury. *Brain*. 2018;141(7):1963–1980.
59. Husain S, Ahmad A, Singh S, Peterseim C, Abdul Y, Nutaitis MJ. PI3K/Akt pathway: a role in delta-opioid receptor-mediated RGC neuroprotection. *Invest Ophthalmol Vis Sci*. 2017;58(14):6489–6499.
60. Halestrap AP, Meredith D. The SLC16 gene family-from monocarboxylate transporters (MCTs) to aromatic amino acid transporters and beyond. *Pflugers Arch*. 2004;447(5):619–628.
61. Halestrap AP. The monocarboxylate transporter family–Structure and functional characterization. *IUBMB Life*. 2012;64(1):1–9.
62. Wilson MC, Meredith D, Fox JE, Manoharan C, Davies AJ, Halestrap AP. Basigin (CD147) is the target for organomercurial inhibition of monocarboxylate transporter isoforms 1 and 4: the ancillary protein for the insensitive MCT2 is EMBIGIN (gp70). *J Biol Chem*. 2005;280(29):27213–27221.
63. Kirwan RP, Fenerty CH, Crean J, Wordinger RJ, Clark AF, O'Brien CJ. Influence of cyclical mechanical strain on extracellular matrix gene expression in human lamina cribrosa cells in vitro. *Mol Vis*. 2005;11:798–810.
64. Murray CM, Hutchinson R, Bantick JR, et al. Monocarboxylate transporter MCT1 is a target for immunosuppression. *Nat Chem Biol*. 2005;1(7):371–376.
65. Nilsson R, Jain M, Madhusudhan N, et al. Metabolic enzyme expression highlights a key role for MTHFD2 and the mitochondrial folate pathway in cancer. *Nat Commun*. 2014;5:3128.
66. Visentin M, Zhao R, Goldman ID. The antifolates. *Hematol Oncol Clin North Am*. 2012;26(3):629–648, ix.
67. Tedeschi PM, Vazquez A, Kerrigan JE, Bertino JR. Mitochondrial methylenetetrahydrofolate dehydrogenase (MTHFD2) overexpression is associated with tumor cell proliferation and is a novel target for drug development. *Mol Cancer Res*. 2015;13(10):1361–1366.
68. Hensley CT, Wasti AT, DeBerardinis RJ, Glutamine and cancer: cell biology, physiology, and clinical opportunities. *J Clin Invest*. 2013;123(9):3678–3684.
69. Hu W, Zhang C, Wu R, Sun Y, Levine A, Feng Z. Glutaminase 2, a novel p53 target gene regulating energy metabolism and antioxidant function. *Proc Natl Acad Sci U S A*. 2010;107(16):7455–7460.
70. Liu J, Zhang C, Lin M, et al. Glutaminase 2 negatively regulates the PI3K/AKT signaling and shows tumor suppression activity in human hepatocellular carcinoma. *Oncotarget*. 2014;5(9):2635–2647.
71. Katt WP, Lukey MJ, Cerione RA. Starving the devourer: cutting cancer off from its favorite foods. *Cell Chem Biol*. 2019;26(9):1197–1199.